HAL
open science

Characterizing mechanical properties of epithelial monolayers based on indentation

Jing-Yi Li, Peng-Cheng Chen, Shao-Zhen Lin, Bo Li

To cite this version:

Jing-Yi Li, Peng-Cheng Chen, Shao-Zhen Lin, Bo Li. Characterizing mechanical properties of epithelial monolayers based on indentation. The European Physical Journal. Special Topics, 2023, 232 (16), pp.2727-2738. 10.1140/epjs/s11734-023-00931-4 . hal-04413810

HAL Id: hal-04413810

https://hal.science/hal-04413810

Submitted on 24 Jan 2024

HAL is a multi-disciplinary open access archive for the deposit and dissemination of scientific research documents, whether they are published or not. The documents may come from teaching and research institutions in France or abroad, or from public or private research centers.

L'archive ouverte pluridisciplinaire **HAL**, est destinée au dépôt et à la diffusion de documents scientifiques de niveau recherche, publiés ou non, émanant des établissements d'enseignement et de recherche français ou étrangers, des laboratoires publics ou privés.

Characterizing mechanical properties of epithelial monolayers based on indentation

Jing-Yi Li[a], Peng-Cheng Chen[a], Shao-Zhen Lin[b,*], and Bo Li[a,*]

[a] *Institute of Biomechanics and Medical Engineering, Applied Mechanics Laboratory, Department of Engineering Mechanics, Tsinghua University, Beijing 100084, China*

[b] *Aix Marseille Univ, Université de Toulon, CNRS, CPT, Turing Centre for Living systems, Marseille UMR 7332, France*

Abstract

Epithelial tissues have a variety of functions such as protection, secretion and absorption. Appropriate mechanical properties of epithelia are essential to achieve these functions. Based on the indentation technology, we combine experiments, theory, and simulations to characterize the mechanical properties of epithelial monolayers. We measure the Young's modulus of *in vitro* cultured epithelial cell monolayers, including MCF-10A human breast epithelial (MCF-10A) cell monolayers and Madin-Darby Canine Kidney (MDCK) cell monolayers. It shows that the elastic moduli of the two kinds of cell monolayers (~1 MPa) have the orders of magnitude larger than those of the constituent cells (~1 kPa) in an isolated state, suggesting a critical role of intercellular interactions via cell–cell junctions in contributing to tissue stiffness. We also find that the elastic modulus of epithelial cell monolayers increases non-linearly with the cell density: MCF-10A cell monolayers exhibit a sharp increase in modulus beyond a critical cell density of ~3000 mm^{-2}, indicating a fluid-to-solid transition as the cell density increases. Our findings reveal the significant contribution of cell density and intercellular interactions to the mechanical properties of epithelial tissues, and could provide mechanical insights into the tissue stiffness changes involved in embryo or tumor development.

Keywords: epithelial tissue; cell monolayer; indentation; elastic modulus

* Corresponding authors: shaozhen.lin@univ-amu.fr (S.Z. Lin) and libome@tsinghua.edu.cn (B. Li)

Introduction

Much has been understood about the mechanical properties of single cells and their changes during physiological and pathological processes, based on a variety of experimental techniques including micropipette aspiration [1], optical tweezers [2], magnetic tweezers [3] and atomic force microscopy (AFM) [4]. However, cells rarely exist as isolated ones in living organisms. Instead, they are usually organized into sheets or clusters to form tissues, through cell–cell junctions [5]. Among them, the simplest tissue is a quasi-two-dimensional structure composed of a monolayer of closely packed cells. As the most common cell monolayer in living organisms, epithelial tissues widely exist on the outer surfaces of various organs in the digestive, respiratory and reproductive systems, and on the inner surfaces of tubular structures such as blood vessels and secretory ducts of glands. Despite their simple structures, epithelial tissues act as crucial physical barrier, secretory or absorption channel, cover the surface of other tissues and are in direct contact with the external environments, thus bearing large mechanical loads and deformations. For example, the alveoli composed of epithelial monolayer undergoes periodic deformations during respiration; the intestinal epithelium is subjected to stretching deformations during intestinal peristalsis; and the inner surface of blood vessels is exposed to fluid shear stress.

Appropriate mechanical properties of epithelial tissues are essential to ensure the normal physiological functions, while abnormal mechanical properties can lead to diseases [6, 7]. Cells can actively change their mechanical properties by cytoskeleton reorganization in response to external mechanical stimulations [8–11]. A variety of pathological processes are usually accompanied by the dysfunction of cytoskeleton, which thus leads to changes in mechanical properties of cells and tissues at both cellular level and tissue level. For instance, at the cellular level, malaria-infected red blood cells show abnormally high stiffness [12]. The stiffness of cancerous cells is roughly an order of magnitude lower than that of normal cells [13]. At the tissue level, mesenchymal stem cell monolayers commonly exhibit higher stiffness than epithelial cell monolayers [14]. Tissue sclerosis is a hallmark of many diseases including pulmonary fibrosis, liver cirrhosis and arteriosclerosis [15]. Therefore, characterizing the mechanical properties of cell monolayers could not only deepen our understanding of various physiological and pathological processes such as embryo development, tissue morphogenesis and tumor invasion, but also provide a mechanical basis for disease diagnosis and tissue

engineering. However, the mechanical properties of cell monolayers are quite different from and cannot be inferred from those of isolated cells due to intercellular interactions.

In this study, we propose an experimental protocol to characterize the mechanical properties of epithelial cell monolayers using the indentation technology. We develop a theoretical model, which accounts for both the bending deformation and the contact deformation, to describe the mechanical response of a cell monolayer under indentation. The Young's modulus of Madin-Darby Canine Kidney (MDCK) cell monolayers and MCF-10A human breast epithelial (MCF-10A) cell monolayers are characterized. It shows that the Young's modulus of cell monolayers is associated with cell density and cell–cell junctions, where the higher cell density and tighter cell–cell junctions lead to a higher Young's modulus.

Materials and methods

The mechanical properties of free-suspended cell monolayers have been studied previously [16]. However, the removal of the extracellular matrix (ECM) may lead to significant changes in the state of cell monolayers, e.g., cell–ECM adhesions. In order to characterize the mechanical properties of cell monolayers under conditions closer to normal physiological conditions, we design an experimental scheme as shown in Fig. 1(a). We first prepare collagen scaffold on perforated glass sheet and then culture cells on it. We characterize the mechanical properties of the composite bilayer formed by cells and collagen after cells reaching confluence. Afterwards, we remove cells by trypsin digestion and characterize the mechanical properties of the collagen monolayer through indentation again. With this experimental scheme, we can infer the mechanical properties of the cell monolayer, based on the directly measured mechanical properties of the collagen monolayer and the composite bilayer.

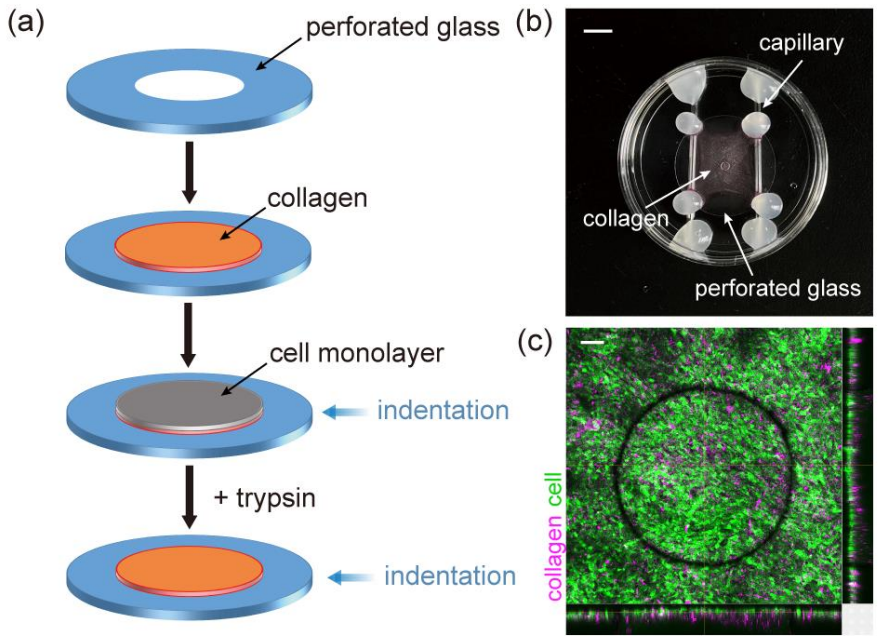

Fig. 1 Experimental setup for the measurement of mechanical properties of cell monolayers. (a) Schematic diagram of the experimental scheme. (b) The experimental device. Scale bar = 5 mm. (c) Fluorescence image of a MDCK cell monolayer cultured on collagen scaffold, with cross-sectional views. Scale bar = 200 μm.

Device assembly

We design perforated glass sheets with inner and outer diameters of 1.5 mm and 18 mm, respectively, and a thickness of 200 μm for cell monolayer preparation. Considering the adaptability with the microscope, the special experimental device is assembled based on Petri dishes of size 35 mm in diameter. Firstly, glass capillary with outer diameter of 1 mm is cut into small segments with a length of 30 mm. Two of these segments are placed in the dish, parallel to each other with a distance of approximately 10 mm, and fixed with hot glue at both ends. After that, we place the perforated glass sheet on the capillary and fix it with hot glue. An example of the experimental device is shown in Fig. 1(b).

Preparation of the collagen scaffold

The collagen gel solution is prepared on ice by mixing collagen type 1A, sterile water, 5× DMEM and collagen reconstitution buffer in a ratio of 5:2:2:1 [17]. The collagen reconstitution buffer is made by dissolving 500 μL of 1 M NaOH solution, 2 mL of 1 M HEPES and 0.22 g $NaHCO_3$ in 10 mL of sterile water. To quantify the

thickness of the collagen monolayer, fluorescent microbeads are added to the prepared collagen gel solution in a ratio of 1:1000 and vortexed for 2 minutes to make them uniformly dispersed in the collagen gel solution. Note that in the preparation of the collagen gel solution, the reagents must be added in the correct order and mixed thoroughly. The collagen gel solution should be freshly prepared before each experiment.

After the preparation of the collagen gel solution, we use a 200-μL pipette tip to aspirate 150 μL of the collagen gel solution and generate a droplet suspended on the hole of the glass sheet. In order to form a more complete cell monolayer, we spread the collagen gel solution on the unperforated part of the glass sheet as well. Then, we carefully move the device to a cell incubator (37°C) for 3–4 hours. The scaffold will be gradually dried and appears thin and flat on the glass sheet, as shown in Fig. 1(b).

Cell culture on devices

We use Madin-Darby Canine Kidney (MDCK) cells and MCF-10A human breast epithelial cells (MCF-10A) in our experiments. These two kinds of cells are cultured at 37°C in an atmosphere of 5% CO_2 in air. The medium of MDCK cells is DMEM supplemented with 10% (vol/vol) FBS and 1% (vol/vol) penicillin-streptomycin. The medium of MCF-10A cells is DMEM/F12 supplemented with 5% (vol/vol) HS, 1% (vol/vol) penicillin-streptomycin, 10 μg/mL insulin, 10 ng/mL EGF, 100 ng/mL cholera toxin and 0.5 μg/mL hydrocortisone.

Before seeding cells, we first add the corresponding medium to the Petri dish until the collagen scaffold is completely submerged. Cells are then peeled off from the bottom of the culture dish using trypsin-EDTA, then centrifuged (5 minutes at 1000 rpm at room temperature) and resuspended to a concentration of 4 million cells per mL using the culture medium. Approximately 4×10^5 cells (100 μL) are placed onto the top of the collagen scaffold and incubated under normal growing conditions until they reach confluence, covering the whole top of the scaffold, which takes approximately 48 h. The confluent cell monolayer grown on collagen scaffold is shown in Fig. 1(c).

Force measurement

We use Piuma Nanoindenter (Optics11 Life, Amsterdam, The Netherlands) for indentation experiments and adopt displacement loading mode. To avoid excessive displacement that may lead to contact between the probe base and the sample and cause damage to the probe, the maximum displacement is set to 10 μm. We have verified that

the maximum displacement of 10 μm is sufficient for the measurement of the linear elastic mechanical properties. Further, we control the strain rate ranging from 3.56×10^{-6} s^{-1} to 1.78×10^{-5} s^{-1} by adjusting loading time, and the results show that strain rate has little effect on the indentation response of samples. The loading time is finally set as 20 seconds and the corresponding strain rate is 4.44×10^{-6} s^{-1}.

We first characterize the composite bilayer consisting of cell monolayer and collagen scaffold by indentation. Then, the samples are incubated with trypsin to remove cells, the incubation time is 30–45 minutes for MCF-10A cells and 120–150 minutes for MDCK cells. The remaining collagen monolayer will be characterized by indentation again to decouple its effect. The processing and analysis of experimental data is performed in MATLAB (Mathworks, Natick, MA, USA).

Theoretical model

Theoretical model for indentation response of homogeneous monolayers

We show the model sketch of the indentation test for freestanding circular film under clamped boundary condition in Fig. 2(a). There are mainly two kinds of classic theoretical models to describe the indentation response, including the membrane model and the plate model. The membrane model assumes that flexural rigidity is negligible compared to tensile rigidity, and thus the deformation is dominated by stretching. Begley and Mackin [18] proposed an analytical expression to describe the indentation response of a clamped circular membrane with a frictionless spherical indenter. Assuming an incompressible layer without pre-stretches, the load–deflection relationship reads

$$u_{\mathrm{s}} = R\left(\frac{a}{R}\right)^{3/4}\left(\frac{16F}{9\pi EhR}\right)^{1/3}, \tag{1}$$

where u_{s} is the deflection at the center of the membrane, F is the load exerted by the indenter, R is the radius of the indenter, h and a are the thickness and the radius of the membrane, and E is the Young's modulus of the membrane. In contrast, the plate model ignores the effect of stretching and focuses on the bending deformation. Based on the Kirchhoff-Love plate theory, the load–deflection relationship reads

$$u_{\mathrm{b}} = \frac{3\left(1-\nu^2\right)a^2}{4\pi Eh^3}F, \tag{2}$$

for clamped boundary conditions, and

$$u_{\mathrm{b}} = \frac{3\left(1-\nu^2\right)a^2}{4\pi E h^3}\frac{\nu+3}{\nu+1}F\,, \tag{3}$$

for simply supported boundary conditions, respectively. Here, ν is the Poisson's ratio of the plate. In addition, Scott et al. [19] demonstrated that the penetration depth of the indenter into the film may be comparable with the overall deflection of the film for soft materials. Thus, the deformation due to contact cannot be ignored.

Here, we consider all these effects, including stretching, bending and contact deformations. We propose a spring model to describe the indentation response of free-suspended monolayers, as shown in Fig. 2 (b). In order to quantify the contributions of bending and stretching in the indentation response, Komaragiri et al. [20] proposed a dimensionless parameter in the case of zero pre-stretch as

$$\lambda = \left[12\left(1-\nu^2\right)\right]^3\left(\frac{Fa^2}{Eh^4}\right)^2. \tag{4}$$

Begley et al. [18] showed that for a circular film with clamped boundary and subjected to a point load at its center, when $\lambda < 85$, bending deformation dominates; while when $\lambda > 3\times10^4$, stretching deformation dominates.

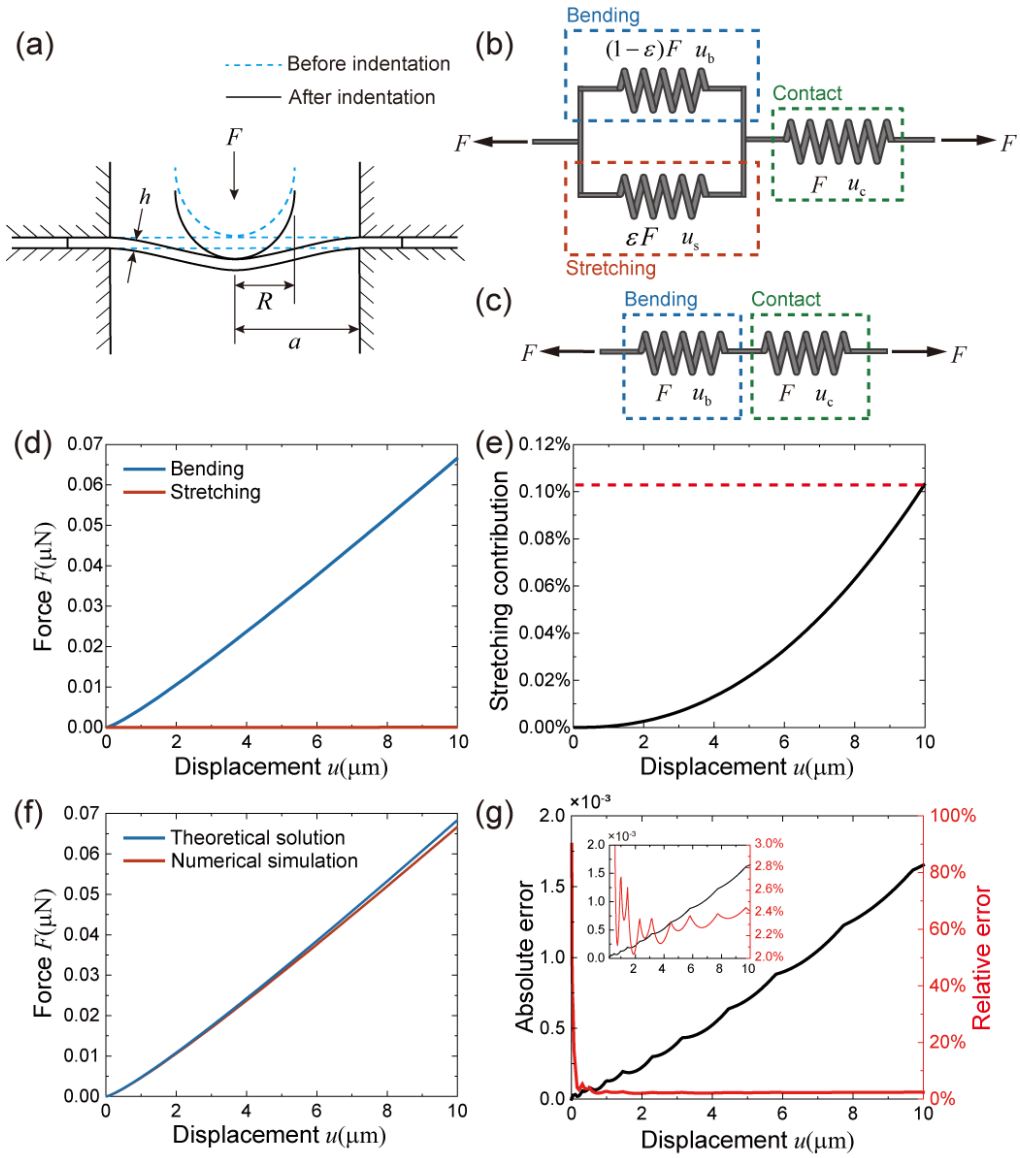

Fig. 2 Theoretical model to describe the indentation response of monolayers and numerical verification. (a) Schematic diagram of the indentation test for freestanding films. (b) Spring model to describe the indentation response of a homogeneous monolayer. Here, ε represents the contribution of stretching during indentation, u_s, u_b and u_c represent the displacement caused by stretching, bending and contact, respectively. (c) Simplified spring model to describe the indentation response of a homogeneous monolayer. (d) Comparison of the contributions of the bending deformation and the stretching deformation to the total forces during indentation. (e) Contribution of the stretching deformation during indentation. (f) Comparison of the indentation response curves predicted by theoretical model and by numerical simulation. (g) Dependence of error due to model simplification on displacement. The inset is the curve after removing data near the origin.

~~It can be seen from Eqs. (1)—(3) that the proportional relationship between the load *F* and the Young's modulus *E* is determined by the physical parameters listed in Table 1 for a given displacement, whether in the membrane model or in the plate model. Therefore, we can determine the *F*–*E* relationship in our experiments with the help of numerical simulations. In our experiments,~~By numerical simulations using the parameters listed in Table 1, we can estimate the dimensionless parameter $\lambda_{\exp} = 102.62$ at the displacement of 10 μm. Thus neither bending deformation nor stretching deformation can be simply ignored. However, we notice that this value is very close to the critical value below which the stretching deformation can be ignored, and our experimental condition is not exactly the same as Begley et al. [18]. We thus employ numerical methods to verify whether the stretching deformation can be neglected to simplify the analytical solution. The numerical simulations are performed in ABAQUS (Dassault Systèmes Simulia Corp., Providence, RI, USA). The comparison between bending force and stretching force at different displacements is shown in Fig. 2(d). It shows that the contribution of stretching increases with the increase of displacement, but the maximum value is only about 0.1% (Fig. 2(e)), which is negligible compared with that of bending. Combining the above analysis, we next ignore the stretching deformation during indentation and simplify the model to two connected springs in series, which involves only bending and contact deformations, as shown in Fig. 2(c). Therefore, we superimpose the classical Hertz solution [21] and the load–deflection relationship obtained by the plate model to establish an analytical solution describing the indentation response of free-suspended monolayers with clamped boundary as

$$u_{\mathrm{cla}} = u_{\mathrm{c}} + u_{\mathrm{b}} = \left[\frac{3\left(1-\nu^2\right)}{4E\sqrt{R}}\right]^{2/3} F^{2/3} + \frac{3\left(1-\nu^2\right)a^2}{4\pi E h^3} F\,, \tag{5}$$

where $u_{\mathrm{c}} = \left[3\left(1-\nu^2\right)/4E\sqrt{R}\right]^{2/3} F^{2/3}$ is the classical Hertz solution for the contact deformation of a semi-infinite elastic medium penetrated by a rigid spherical indenter, assuming frictionless contact. Similarly, the analytical solution for monolayers with simply supported boundary is formulated as

$$u_{\mathrm{ssp}} = u_{\mathrm{c}} + u_{\mathrm{b}} = \left[\frac{3\left(1-\nu^2\right)}{4E\sqrt{R}}\right]^{2/3} F^{2/3} + \frac{3\left(1-\nu^2\right)a^2}{4\pi E h^3}\frac{\nu+3}{\nu+1}F \ . \tag{6}$$

We next examine the model simplification error. The concentrated force assumption is introduced in the derivation of analytical solution of plate model, while the indenter size is finite in the experiments. For a given displacement under clamped boundary condition, we compare the force calculated by the point load analytical solution with that given by the numerical simulation using a finite-sized indenter, as shown in Fig. 2(f) and 2(g). The results show that the load–deflection curves given by analytical solution and numerical simulation are essentially the same, and the relative error is about 2.5% at a displacement of 10 μm, at an acceptable level. This indicates that our model simplification has quite weak impact on the accuracy of the results, and the analytical solution given by Eqs. (5) and (6) can be used to analyze the experimental data of monolayer indentation.

In addition, the above analytical solutions are derived based on clamped or simply supported boundary conditions, while the boundary condition in our experimental system is not strictly consistent with these two types of boundary conditions, as shown in Fig. 3(a). Meanwhile, the results of numerical simulations indicate that the boundary condition has a remarkable impact on the indentation response curve, as shown in Fig. 3(b). We fit the data obtained from numerical simulations with the analytical solutions of monolayer indentation under clamped or simply supported boundary conditions, respectively, as shown in Fig. 3(c). Our analytical solution can well fit the data under the corresponding boundary conditions. However, neither of the two types of theoretical solutions can provide a good fit to the data obtained under the actual boundary condition. Therefore, it is necessary to correct the experimental data before analyzing them with the above theoretical solution.

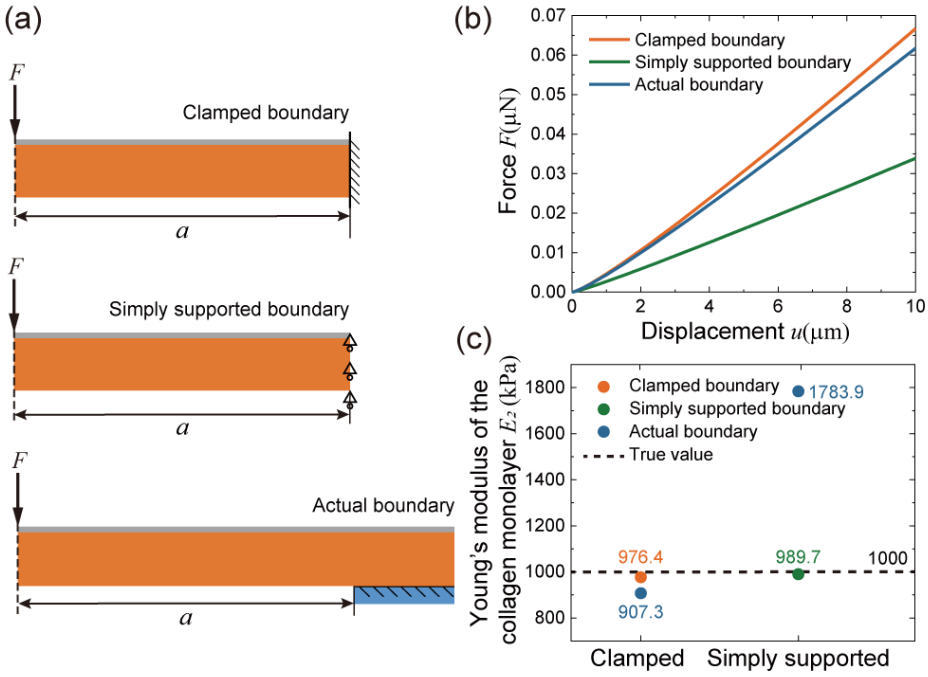

Fig. 3 Effect of boundary conditions. (a) Schematics of different boundary conditions: (top) clamped boundary; (middle) simply supported boundary; (bottom) actual boundary. The bottom of the sample is fixed to the glass sheet outside the indentation area. (b) Indentation response curves obtained by numerical simulations under different boundary conditions. (c) The Young's modulus fitted by theoretical solutions with indentation data from clamped, simply supported or actual boundary conditions shown in (b). The horizontal axis represents the theoretical solution taken in the fit for clamped boundary conditions (Eq. (5)) and simply supported boundary conditions (Eq. (6)), respectively.

Theoretical model for indentation response of composite bilayers

For the composite bilayer system, we assume that the individual layers are isotropic materials and there is no relative sliding. The load–deflection relationship of the circular composite plate subjected to concentrated force at its center under clamped boundary can be calculated using the transformed rigidity proposed by Pister et al. [22] as

$$u_{\mathrm{b}} = \frac{3\left(1-\nu^{2}\right)a^{2}}{4\pi E_{\mathrm{b}}\left(h_{1}+h_{2}\right)^{3}}F\,, \tag{7}$$

$$E_{\mathrm{b}}=\frac{E_1^{\,2}h_1^{\,4}+4E_1E_2h_1^{\,3}h_2+6E_1E_2h_1^{\,2}h_2^{\,2}+4E_1E_2h_1h_2^{\,3}+E_2^{\,2}h_2^{\,4}}{\left(h_1+h_2\right)^3\left(E_1h_1+E_2h_2\right)}, \tag{8}$$

where h_1, E_1 and h_2, E_2 are the thickness or the Young's modulus of the top and bottom layer, respectively, and E_{b} is the effective bending Young's modulus of the composite bilayer system. We further assume that the Poisson's ratio of the top and bottom layers are the same, $\nu_1=\nu_2=\nu$.

For Hertzian indentation on coating/substrate systems, Hsueh et al. [23] proposed the effective contact Young's modulus as

$$E_{\mathrm{c}}=\alpha E_1, \tag{9}$$

where α is formulated as

$$\alpha=\left\{1+\left[\frac{E_1\left(1+\nu\right)}{\pi E_2\left(1-\nu^2\right)}-\frac{1}{\pi\left(1-\nu\right)}\right]\left[\left(3-2\nu\right)\lambda_1+\lambda_2\right]\right\}^{-1}. \tag{10}$$

λ_1 and λ_2 are functions of h_1/r_{c}, given by

$$\lambda_1=\frac{\pi}{2}\left(1+\frac{h_1^{\,2}}{r_c^{\,2}}\right)-\frac{h_1}{r_c}-\left(1+\frac{h_1^{\,2}}{r_c^{\,2}}\right)\sin^{-1}\left[\frac{h_1}{r_c}\left(1+\frac{h_1^{\,2}}{r_c^{\,2}}\right)^{-1/2}\right], \tag{11}$$

$$\lambda_2=-\frac{\pi}{2}\left(1+\frac{3h_1^{\,2}}{r_c^{\,2}}\right)+\frac{3h_1}{r_c}+\left(1+\frac{3h_1^{\,2}}{r_c^{\,2}}\right)\sin^{-1}\left[\frac{h_1}{r_c}\left(1+\frac{h_1^{\,2}}{r_c^{\,2}}\right)^{-1/2}\right], \tag{12}$$

where r_{c} is the radius of the contact area. Assuming a rigid spherical indenter and a semi-infinite elastic medium, the contact radius is calculated as [24]

$$r_{\mathrm{c}}=\sqrt{Ru_{\mathrm{c}}} \tag{13}$$

We assume that the contact radius can be calculated in the same way for coating/substrate systems. Replacing the Young's modulus in classical Hertz solution with Eq. (9), we obtain the modified Hertzian solution for coating/substrate systems,

$$u_{\mathrm{c}}=\left[\frac{3\left(1-\nu^2\right)}{4E_{\mathrm{c}}\sqrt{R}}\right]^{2/3}F^{2/3}. \tag{14}$$

We next superimpose Eqs. (7) and (14) to establish a theoretical solution for composite bilayers under clamped boundary conditions as

$$u_{\mathrm{cla}}=u_{\mathrm{c}}+u_{\mathrm{b}}=\left[\frac{3\left(1-\nu^2\right)}{4E_{\mathrm{c}}\sqrt{R}}\right]^{2/3}F^{2/3}+\frac{3\left(1-\nu^2\right)a^2}{4\pi E_{\mathrm{b}}\left(h_1+h_2\right)^3}F=k_{\mathrm{c}}F^{2/3}+k_{\mathrm{b}}F, \tag{15}$$

where k_c and k_b are the coefficients of two terms, respectively. In order to apply this model, we need two parameters, the ratio of the Young's modulus E_1 / E_2, and the ratio of the thickness of the cell monolayer to the contact radius h_1 / r_c. It can be seen from Eq. (13) that the contact radius is related to displacement, which means that the correction factor α of the effective contact Young's modulus E_c takes different values at different displacements. Thus we adopt the process shown in Fig. 4(a) to apply the above analytical solution.

The displacement and force data are obtained experimentally. We start the data analysis with the indentation data of the collagen monolayer, which leads to the measurement of the Young's modulus of the collagen monolayer E_2. We further assume an appropriate value of the Young's modulus of the cell monolayer E_1. For each point, the contact radius can be calculated by Eq. (13), and the two coefficients for theoretical solution k_b and k_c can be obtained by substituting other known values. Then, we substitute the force data into Eq. (15) to calculate the fitted displacement $\hat{u}_i$ and the residual. Finally, we adjust the hypothesis on the Young's modulus of the cell monolayer based on the residual sum of squares ε, and choose E_1 that minimizes ε as the fitted value of the Young's modulus of the cell monolayer.

We verify the above data analyzing method by numerical simulations. In the simulations, we set the Young's modulus of the collagen monolayer as $E_2 = 1\,\text{kPa}$ and change the Young's modulus of the cell monolayer to obtain several data sets under different ratio of the Young's modulus. Then, the data obtained by numerical simulations are analyzed with the procedure described above, where the input value of E_2 is set as the true value 1 kPa. As shown in Fig. 4(b), the fitting error of the Young's modulus of the cell monolayer gradually increases as the ratio of the Young's modulus increases; the relative error between the fitted value and the true value is close to 70% when E_1 / E_2 reaches 20. To ensure the accuracy of the theoretical model, we use this analytical solution only when E_1 / E_2 is less than 10.

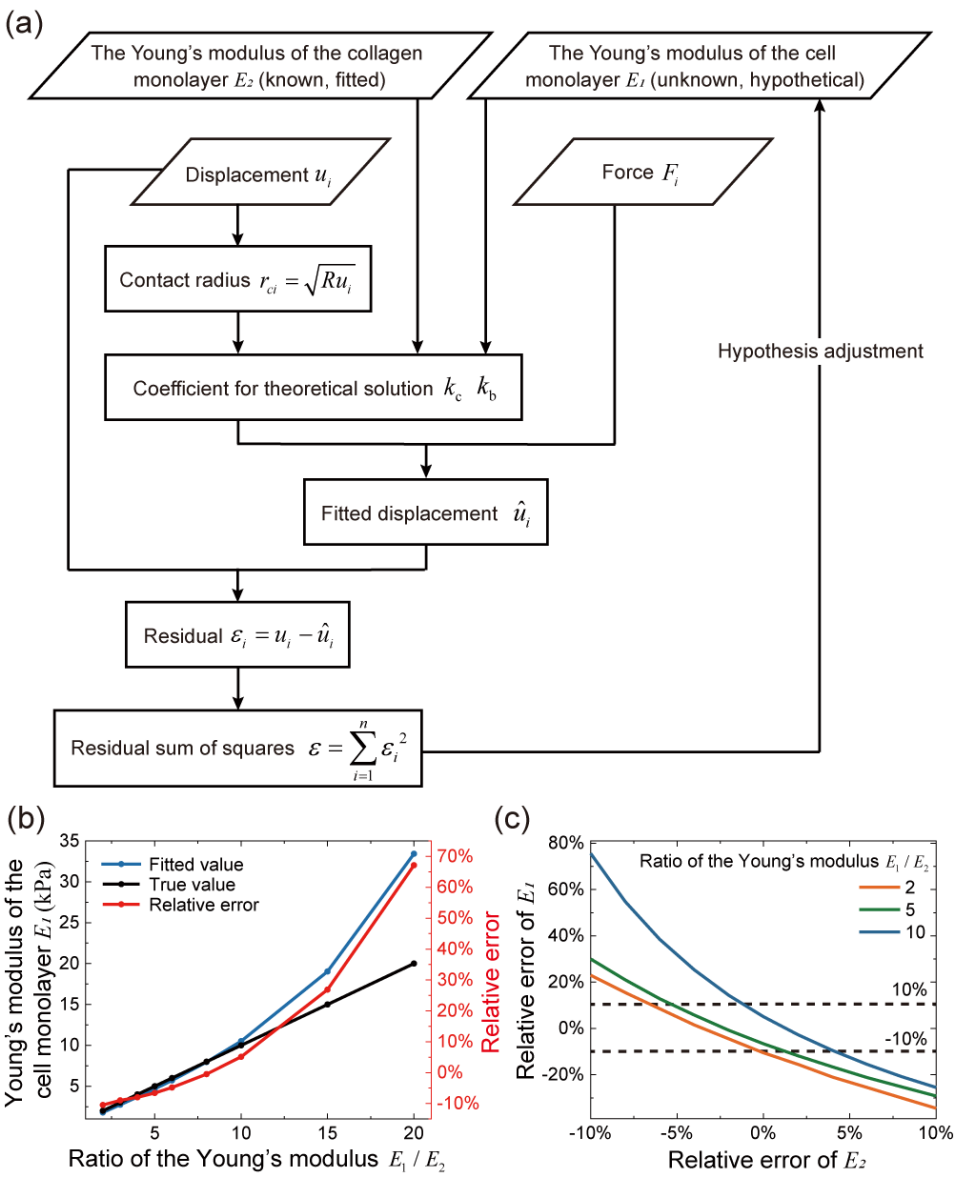

Fig. 4 Computational procedure and error analysis of the theoretical model describing indentation response of bilayers. (a) Flow chart of the application of theoretical solution for bilayer indentation to determine the Young's modulus of a cell monolayer. (b) Dependence of the Young's modulus of a cell monolayer calculated by theoretical solution and its relative error on the ratio of the Young's modulus of a bilayer. (c) Dependence of the Young's modulus fitting error of a cell monolayer on that of a collagen monolayer, under different ratio of the Young's modulus of the bilayer.

In addition, we further verify the effect of fitting error of E_2 on fitting error of E_1. Here, we change the input value of E_2 in the same procedure and analyze the data obtained by numerical simulations again. As shown in Fig. 4(c), we find that the fitted

value of E_1 is sensitive to the fitting error of E_2 and the relationship between these two factors is related to the ratio of the Young's modulus. It is better to keep the fitting error of E_2 within 5% to ensure the fitting error of E_1 less than 10%.

Results

We first analyze the force–displacement data of the collagen monolayer obtained by indentation, as shown in Fig. 5(a). We have shown that the analytical solution under clamped or simply supported boundary condition cannot provide a good fit to the experimental data. We next correct our experimental data by data obtained under clamped boundary conditions. The ratio of the force obtained under these two boundary conditions at the same displacement is taken logarithmically and then fitted linearly to obtain the boundary condition correction formula as

$$F_{\mathrm{cla}} = 1.0564 \times u^{0.009482} \times F_{\mathrm{exp}} . \tag{16}$$

Note that we focus on the Young's modulus, which is obtained in the linear elastic region and the theoretical model is derived under the assumption of linear elasticity. However, the collagen monolayer exhibits nonlinear force–displacement relationship as the displacement increases. Thus we fit the experimental data with the theoretical model to check whether it is in the linear elastic region, and only select the data with great linearity (with the coefficient of determination $R^2 > 0.99$) for analysis. We analyze the experimental data with the theoretical solution describing indentation response of monolayers given by Eq. (5). The values of the parameters in the formula are set to be consistent with the real condition, as shown in Table 1. The Young's modulus of collagen monolayers fitted by Eq. (5) are shown in Table 2 and Fig. 5(b).

Table 1 List of the physical parameters in our experiments

Physical meaning	Symbol	Value
Poisson's ratio of collagen monolayers	ν	0.5
Radius of the indenter	R	49 μm
Radius of the indentation area	a	750 μm
Thickness of collagen monolayers	h_2	100 μm

Table 2 Young's modulus of collagen monolayers E_2

Cell type	Serial number	Young's modulus of the collagen monolayer (kPa)	Mean ± SD (kPa)
MDCK	1	13.19	12.15 ± 1.88
	2	10.40	
	3	14.26	
	4	10.75	
MCF-10A	1	25.30	25.94 ± 2.99
	2	26.50	
	3	30.63	
	4	27.62	
	5	26.81	
	6	21.39	
	7	23.33	

Our experimental analysis shows that the Young's modulus of collagen monolayers cultured with the same type of cells do not exhibit significant differences, as shown in Fig. 5(b). This indicates that the mechanical property of collagen monolayers is relatively stable. We also find that collagen monolayers cultured with MCF-10A cells exhibit significantly higher Young's modulus, which may be caused by the difference in the form of interaction between different types of cells and the ECM.

Based on the fitted Young's modulus of collagen monolayers, we next analyze the force–displacement data of the composite bilayer using the procedure described in Fig. 4(a). We show the indentation response curves of the composite bilayer formed by collagen and MDCK cells or MCF-10A cells in Fig. 5(c) and 5(d), respectively. We find that there are obvious groupings in the indentation data of the composite bilayer formed by MCF-10A cells and collagen. Thus, we label them into three groups for the convenience of subsequent discussion.

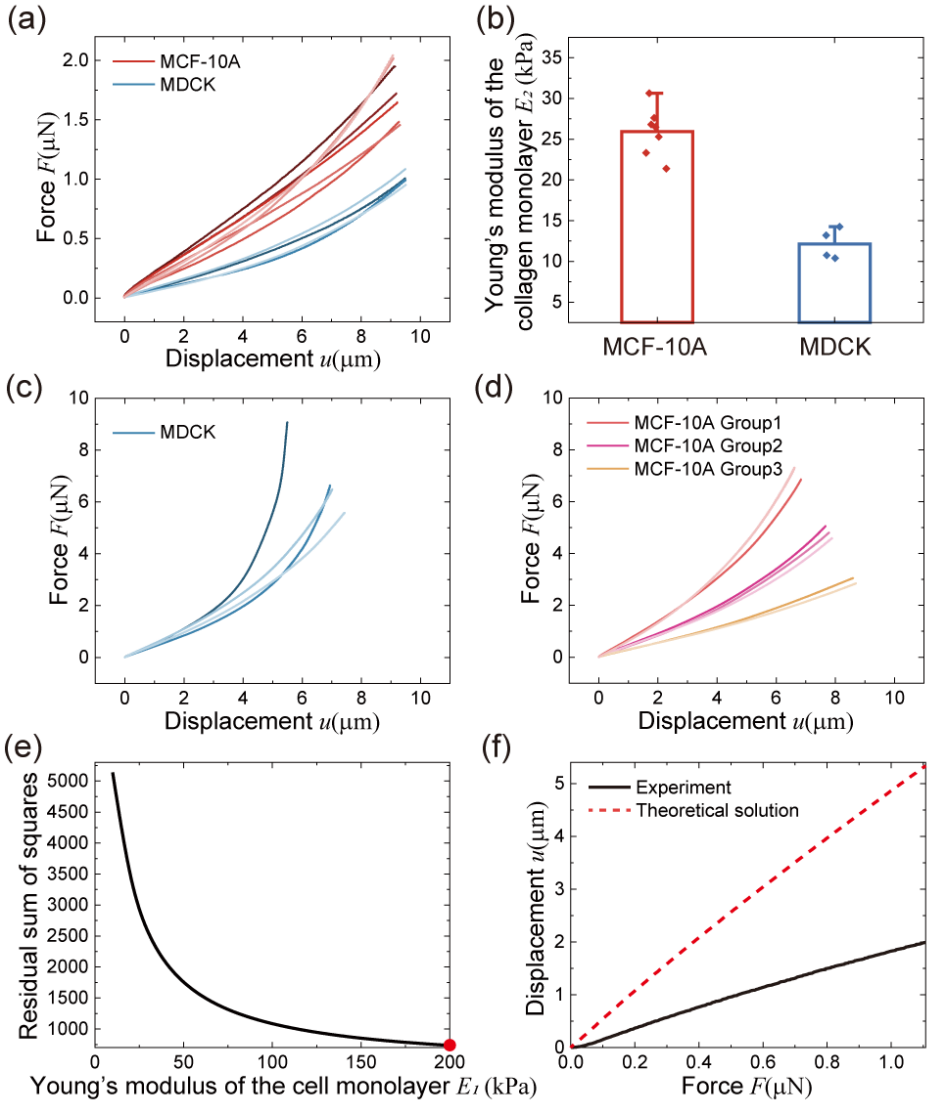

Fig. 5 Mechanical properties of collagen monolayers and preliminary analysis of indentation response of bilayers. (a) Indentation response curves of collagen monolayers. The series of red curves represent collagen monolayers that have been cultured with MCF-10A cells. The series of blue curves represent collagen monolayers that have been cultured with MDCK cells. Each curve is obtained by averaging 5 data sets under the same experimental condition. (b) Young's modulus of collagen monolayers cultured with different types of cells. (c) Indentation response curves of the composite bilayer formed by MDCK cells and collagen. (d) Indentation response curves of the composite bilayer formed by MCF-10A cells and collagen. (e) Dependence of residual sum of squares for data fitting with theoretical solution of bilayer (Eq. (15)) on the hypothetical Young's modulus of the cell monolayer. The red dot represents the Young's modulus of the cell monolayer determined by theoretical model (Eq. (15)). Data shown here are obtained from a representative sample of

the composite bilayer formed by MDCK cells and collagen. (f) The theoretical indentation response curve is obtained by Eq. (15) using the Young's modulus of the cell monolayer determined by theoretical model. It is compared with the indentation response curve obtained by the experiment. Data shown here come from the same experiment as in (e).

For illustration, we take the first sample of composite bilayer formed by MDCK cells and collagen as an example. In this sample, the Young's modulus of the collagen monolayer is 13.19 kPa. We have shown that the fitting error of the Young's modulus of cell monolayers increases with the ratio of the Young's modulus (Fig. 4(b)). Therefore, we set the range of the hypothetical Young's modulus of the cell monolayer to 0–200 kPa in the data analyzing procedure, and the results are shown in Fig. 5(e) and 5(f). We find that the best fitting value for the Young's modulus of the cell monolayer has not been found within the range of 0–200 kPa. This indicates that the ratio of the Young's modulus in our experiments exceeds the applicable range of the theoretical solution. Thus the indentation data obtained by our experiments are not suitable to be analyzed with the theoretical solution.

We next design a new scheme to deal with the indentation data of composite bilayers, as shown in Fig. 6(a). In this new scheme, first, we input the fitted Young's modulus of the collagen monolayer and the hypothetical Young's modulus of the cell monolayer into the FEM (Finite Element Method) model, and perform numerical simulation to obtain the indentation response curve of the composite bilayer. Second, we compare the simulation result with the experimental data and check whether they match well (with the minimal residual sum of squares); if they do not match well, we will adjust the hypothetical value and repeat the above steps until we obtain a good estimate.

We show the fitted value of the Young's modulus of cell monolayers in Table 3. The Young's modulus of cell monolayers not only exhibit a correlation with the cell type, but also exhibit intergroup differences among monolayers composed of the same type of cells, as shown in Fig. 6(b). Based on our experimental observations, we speculate that the difference in the stiffness of cell monolayers is caused by the difference in cell density within the monolayer. To verify this assumption, we count the cell density by cell segmentation, as shown in Table 4. We further show the Young's modulus of cell monolayers as a function of the cell density in Fig. 6(c). It indicates that the difference in cell density can explain the difference in the mechanical properties

of cell monolayers. Furthermore, we find that the Young's modulus of cell monolayers increases with the cell density. This is reminiscent of the previously reported fluid-to-solid transition (or jamming transition) that takes place as a cell monolayer matures and ages, during which the cell monolayer exhibits more solid-like behaviors at higher cell densities [25–27]. Based on the stiffness-versus-cell density curve in Fig. 6(c), our experimental measurements indicate that the MCF-10A cell monolayers may undergo a fluid-to-solid transition at a critical cell density of ~3000 mm^{-2}.

Table 3 Young's modulus of cell monolayers E_1

Cell type	Serial number	Young's modulus of the cell monolayer (MPa)	Mean ± SD (MPa)
MDCK	1	21.38	19.72 ± 2.37
	2	16.57	
	3	19.25	
	4	21.69	
MCF-10A	1	9.25	7.30 ± 2.76
	2	5.35	
	3	0.66	0.67 ± 0.07
	4	0.59	
	5	0.72	
	6	0.29	0.29 ± 0.00
	7	0.29	

Table 4 Cell density within the monolayer

Group	Cell density (mm^{-2})
MDCK	6075
MCF-10A Group1	4250
MCF-10A Group2	2875
MCF-10A Group3	2300

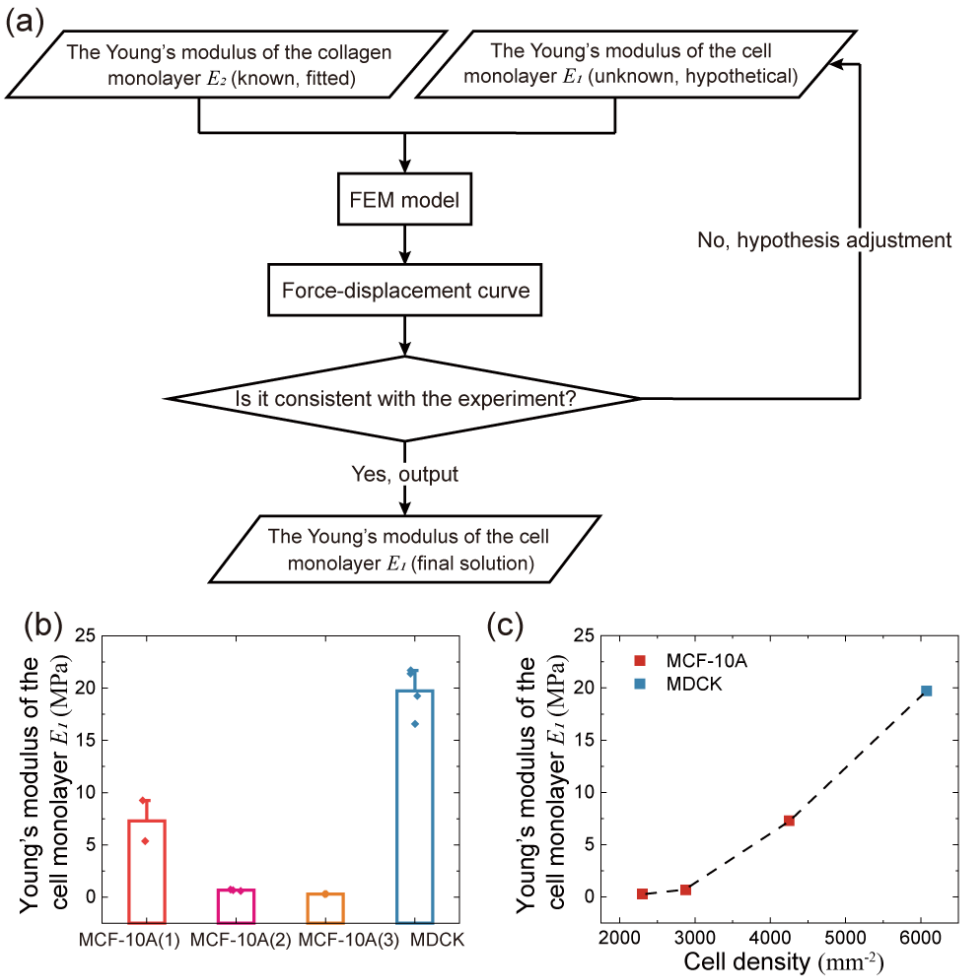

Fig. 6 Mechanical properties of cell monolayers. (a) Flow chart for determining the Young's modulus of cell monolayers with numerical methods. (b) Young's modulus of cell monolayers. (c) The Young's modulus of cell monolayers as a function of the cell density in the monolayer.

We further find that MDCK cell monolayers exhibit a higher stiffness than MCF-10A cell monolayers (Fig. 6(b)). This might be explained by the difference in the cell density, see Fig. 6(c), but one cannot exclude the contribution of difference in cell–cell interactions. Both MDCK cells and MCF-10A cells belong to simple cuboidal epithelia cells, but there are some differences in cell morphology. MDCK cells exhibit regular polygonal morphology at low cell densities, while MCF-10A cells exhibit elongated shape at the same density, and only at high cell densities do they exhibit similar polygonal morphology.

Rother et al. [28] investigated the mechanical properties of isolated cells of different cell lines with AFM, and found that the shear modulus of MDCK cells differed

from that of MCF-10A cells. Assuming isotropic and incompressible material of cells, the Young's modulus of MDCK cells and MCF-10A cells can be estimated as 0.19 kPa and 0.47 kPa, respectively; both are much smaller (orders of magnitude) than those of corresponding cell monolayers. This indicates that intercellular interactions (via cell–cell junctions) contribute critically to the stiffness of cell monolayers. Previous studies have shown that cell–cell junctions play an important role in maintaining the mechanical properties of cell monolayers. Harris et al. [16] treated the cell monolayer with EDTA (Ethylenediaminetetraacetic Acid) to cut off the intercellular interactions and found that the Young's modulus of the monolayer decreased significantly. In our experiments, we find that MCF-10A cell monolayers and MDCK cell monolayers show different responses to trypsin treatment. It takes longer to destroy the cell–cell junctions of MDCK cells, indicating that MDCK cell monolayers form tighter cell–cell junctions than MCF-10A cell monolayers. Therefore, besides the cell density, the difference in intercellular interactions also contribute to the difference in the stiffness of MCF-10A cell monolayers and MDCK cell monolayers.

Conclusions

We have established an experimental system to characterize the Young's modulus of cell monolayers based on the indentation technology, and applied this method to measure the Young's modulus of MDCK cell monolayers and MCF-10A cell monolayers. We propose a theoretical model accounting for bending deformation and contact deformation to describe the indentation response of monolayers, and bilayers, respectively. Our results show that the Young's modulus of cell monolayers is associated with cell density and collective state. A cell monolayer exhibits higher Young's modulus as the cell density increases. Based on measurements of cell motions, previous studies have reported a fluid-to-solid transition of cell monolayers as they mature [25–27]. Our experiments provide a direct evidence on the collective state-dependent stiffness of cell monolayers based on direct measurements of cell monolayers that undergo fluid-to-solid transition. In addition, intercellular interactions via cell–cell junctions are found to contribute critically to tissue stiffness.

Although we have established the theoretical model describing indentation response of the composite bilayer, the proposed model has a relatively narrow applicable range, and the fitting error grows rapidly as the ratio of the Young's modulus increases to large values ($E_1/E_2>10$). We speculate that the error mainly results from

the approximate calculation of the contact radius. In our experiments, the total displacement is composed of bending deformation and contact deformation, and the contact radius only depends on the contact deformation. However, since the exact contribution of contact deformation in the total displacement is unknown, directly using the total displacement to calculate the contact radius will lead to inaccuracy. In addition, Hsueh et al. [23] pointed out that the contact radius for coating/substrate systems cannot be simply calculated using the solution of semi-infinite elastic medium. Further, the contact radius of a rigid spherical indenter loading onto a coating/substrate system is affected by various factors and lacks a simple analytical solution [23]. Therefore, future attempts can be made to measure the contact radius experimentally, and thus broadening the application of the theoretical model and reducing the complexity of data analyzing.

Our results show that the Young's modulus of MDCK and MCF-10A cell monolayers roughly have the order of 1 MPa. This order of magnitude is different from those measured by tensile test [16] or cell monolayer deformation microscopy [14] *in vitro*, which is generally of the order of 1 kPa. However, using the travelling-wave optical coherence elastography technique, Feng et al. [29] measured the Young's modulus of epidermis in male forearm skin as 4.57 ± 0.27 MPa, which is close to our measurement. The reason could lie in that our experimental scheme does not destroy cell–ECM adhesions, and thus the Young's modulus of cell monolayers under conditions closer to normal physiological conditions is obtained. Finally, it should be noted that the cell monolayers in our experiments are different from the *in vivo* state. Nevertheless, since we take the cell–ECM interactions into account, in our method, the state of cell monolayers is more close to the *in vivo* state, as compared to other methods including the tensile test method [16] and the cell monolayer deformation microscopy method [14].

Data availability

The datasets generated and analyzed during the current study are available from the corresponding author on reasonable request.

Statements and declarations

Competing interests

The authors declare that they have no conflict of interest associated with the presented work.

Author contributions

B.L. and P.C.C. conceived the project and designed the research. J.Y.L. and P.C.C. performed the experiments, theoretical modeling and numerical simulations. J.Y.L., P.C.C., S.Z.L., and B.L. analyzed the data. J.Y.L., S.Z.L., and B.L. wrote the paper.

Acknowledgements

Supports from National Natural Science Foundation of China (12272202 and 11921002) are acknowledged.

References

1. W. R. Jones, H. P. Ting-Beall, G. M. Lee, S. S. Kelley, R. M. Hochmuth, F. Guilak, Alterations in the Young's modulus and volumetric properties of chondrocytes isolated from normal and osteoarthritic human cartilage. J. Biomech. 32, 119–127 (1999) https://doi.org/10.1016/S0021-9290(98)00166-3
2. B. Pontes, Y. Ayala, A. C. C. Fonseca, L. F. Romão, R. F. Amaral, L. T. Salgado, F. R. Lima, M. Farina, N. B. Viana, V. Moura-Neto, H. M. Nussenzveig, Membrane elastic properties and cell function. PLoS ONE 8, e67708 (2013) https://doi.org/10.1371/journal.pone.0067708
3. Y. C. Poh, S. Na, F. Chowdhury, M. Ouyang, Y. Wang, N. Wang, Rapid activation of Rac GTPase in living cells by force is independent of Src. PLoS ONE 4, e7886 (2009) https://doi.org/10.1371/journal.pone.0007886
4. E. Moeendarbary, L. Valon, M. Fritzsche, A. R. Harris, D. A. Moulding, A. J. Thrasher, E. Stride, L. Mahadevan, G. T. Charras, The cytoplasm of living cells behaves as a poroelastic material. Nat. Mater. 12, 253–261 (2013) https://doi.org/10.1038/nmat3517
5. U. Schnell, V. Cirulli, B. N. G. Giepmans, EpCAM: structure and function in health and disease. Biochim. Biophys. Acta, Biomembr. 1828, 1989–2001 (2013) https://doi.org/10.1016/j.bbamem.2013.04.018
6. S. E. Cross, Y. S. Jin, J. Rao, J. K. Gimzewski, Nanomechanical analysis of cells from cancer patients. Nat. Nanotechnol. 2, 780–783 (2007) https://doi.org/10.1038/nnano.2007.388
7. Z. Su, Z. Chen, K. Ma, H. Chen, J. W. K. Ho, Molecular determinants of intrinsic cellular stiffness in health and disease. Biophys. Rev. 14, 1197–1209 (2022) https://doi.org/10.1007/s12551-022-00997-9
8. D. A. Fletcher, R. D. Mullins, Cell mechanics and the cytoskeleton. Nature 463, 485–492 (2010) https://doi.org/10.1038/nature08908
9. T. Lecuit, P. F. Lenne, E. Munro, Force generation, transmission, and integration during cell and tissue morphogenesis. Annu. Rev. Cell Dev. Biol. 27, 157–184 (2011) doi: 10.1146/annurev-cellbio-100109-104027
10. J. Z. Kechagia, J. Ivaska, P. Roca-Cusachs, Integrins as biomechanical sensors of the microenvironment. Nat. Rev. Mol. Cell Biol. 20, 457–473 (2019) https://doi.org/10.1038/s41580-019-0134-2

11. N. I. Petridou, Z. Spiró, C. P. Heisenberg, Multiscale force sensing in development. Nat. Cell Biol. 19, 581–588 (2017) https://doi.org/10.1038/ncb3524
12. F. K. Glenister, R. L. Coppel, A. F. Cowman, N. Mohandas, B. M. Cooke, Contribution of parasite proteins to altered mechanical properties of malaria-infected red blood cells. Blood 99, 1060–1063 (2002) https://doi.org/10.1182/blood.V99.3.1060
13. M. Lekka, P. Laidler, D. Gil, J. Lekki, Z. Stachura, A. Z. Hrynkiewicz, Elasticity of normal and cancerous human bladder cells studied by scanning force microscopy. Eur. Biophys. J. 28, 312–316 (1999) https://doi.org/10.1007/s002490050213
14. A. A. Sutton, C. W. Molter, A. Amini, J. Idicula, M. Furman, P. Tirgar, Y. Tao, A. Ghagre, N. Koushki, A. Khavari, A. J. Ehrlicher, Cell monolayer deformation microscopy reveals mechanical fragility of cell monolayers following EMT. Biophys. J. 121, 629–643 (2022) https://doi.org/10.1016/j.bpj.2022.01.003
15. T. R. Cox, J. T. Erler, Remodeling and homeostasis of the extracellular matrix: implications for fibrotic diseases and cancer. Dis. Models Mech. 4, 165–178 (2011) https://doi.org/10.1242/dmm.004077
16. A. R. Harris, L. Peter, J. Bellis, B. Baum, A. J. Kabla, G. T. Charras, Characterizing the mechanics of cultured cell monolayers. Proc. Natl. Acad. Sci. U. S. A. 109, 16449–16454 (2012) https://doi.org/10.1073/pnas.1213301109
17. A. R. Harris, J. Bellis, N. Khalilgharibi, T. Wyatt, B. Baum, A. J Kabla, G. T. Charras, Generating suspended cell monolayers for mechanobiological studies. Nat. Protoc. 8, 2516–2530 (2013) https://doi.org/10.1038/nprot.2013.151
18. M. R. Begley, T. J. Mackin, Spherical indentation of freestanding circular thin films in the membrane regime. J. Mech. Phys. Solids 52, 2005–2023 (2004) https://doi.org/10.1016/j.jmps.2004.03.002
19. O. N. Scott, M. R. Begley, U. Komaragiri, T. J. Mackin, Indentation of freestanding circular elastomer films using spherical indenters. Acta Mater. 52, 4877–4885 (2004) https://doi.org/10.1016/j.actamat.2004.06.043
20. U. Komaragiri, M. R. Begley, J. G. Simmonds, The mechanical response of freestanding circular elastic films under point and pressure loads. J. Appl. Mech. 72, 203–212 (2005) https://doi.org/10.1115/1.1827246
21. K. L. Johnson, Contact mechanics, 1st edn. (Cambridge University Press, Cambridge, 1987)

22. K. S. Pister, S. B. Dong, Elastic bending of layered plates. J. Eng. Mech. Div. 85, 1–10 (1959) https://doi.org/10.1061/JMCEA3.0000100
23. C. H. Hsueh, P. Miranda, Master curves for Hertzian indentation on coating/substrate systems. J. Mater. Res. 19, 94–100 (2004) https://doi.org/10.1557/jmr.2004.19.1.94
24. N. E. Waters, The indentation of thin rubber sheets by spherical indentors. Br. J. Appl. Phys. 16, 557–563 (1965) doi: 10.1088/0508-3443/16/4/321
25. T. E. Angelini, E. Hannezo, X. Trepat, M. Marquez, J. J. Fredberg, D. A. Weitz, Glass-like dynamics of collective cell migration. Proc. Natl. Acad. Sci. U. S. A. 108, 4714–4719 (2011) https://doi.org/10.1073/pnas.1010059108
26. J. A. Park, J. H. Kim, D. Bi, J. A. Mitchel, N. T. Qazvini, K. Tantisira, C. Y. Park, M. McGill, S. H. Kim, B. Gweon, J. Notbohm, R. S. Jr, S. Burger, S. H. Randell, A. T. Kho, D. T. Tambe, C. Hardin, S. A. Shore, E. Israel, D. A. Weitz, D. J. Tschumperlin, E. P. Henske, S. T. Weiss, M. L. Manning, J. P. Butler, J. M. Drazen, J. J. Fredberg, Unjamming and cell shape in the asthmatic airway epithelium. Nat. Mater. 14, 1040–1048 (2015) https://doi.org/10.1038/nmat4357
27. S. Z. Lin, W. Y. Zhang, D. Bi, B. Li, X. Q. Feng, Energetics of mesoscale cell turbulence in two-dimensional monolayers. Commun. Phys. 4, 21 (2021) https://doi.org/10.1038/s42005-021-00530-6
28. J. Rother, H. Nöding, I. Mey, A. Janshoff, Atomic force microscopy-based microrheology reveals significant differences in the viscoelastic response between malign and benign cell lines. Open Biol. 4, 140046 (2014) https://doi.org/10.1098/rsob.140046
29. X. Feng, G. Y. Li, A. Ramier, A. M. Eltony, S. H. Yun, In vivo stiffness measurement of epidermis, dermis, and hypodermis using broadband Rayleigh-wave optical coherence elastography. Acta Biomater. 146, 295–305 (2022) https://doi.org/10.1016/j.actbio.2022.04.030